AIR ENTRAINMENT AND VELOCITY REDISTRIBUTION IN A BOTTOM OUTLET JET FLOW

LUKE TOOMBES [1] and HUBERT CHANSON [2]

[1]Connell Wagner, 433 Boundary St, Spring Hill 4000, Australia; formerly Dept of Civil Engineering, The University of Queensland, Brisbane QLD 4072, Australia
[2]Dept of Civil Engineering, The University of Queensland, Brisbane QLD 4072, Australia
(Tel: +61-7-3365-4163, Fax: +61-7-3365-4599, e-mail: h.chanson@uq.edu.au)

Abstract

This study aims to provide some new understanding of interfacial aeration and velocity redistribution in high-velocity water jets discharging past an abrupt drop. Typical applications include bottom outlets and spillway flows past ski jump. Downstream of the drop, the free-jet entrains air at both upper and lower air-water interfaces, as well as along the sides. At the lower nappe, an air-water shear layer develops and the velocity redistribution within the jet was found to be similar to that in two-dimensional wake flow. The results highlighted further two distinct flow regions. Close to the abrupt drop ($We_X < 5000$), the flow was dominated by momentum transfer. Further downstream ($We_X > 5000$), a strong competition between air bubble diffusion and momentum exchanges developed.

Keywords: Bottom outlet; Interfacial aeration; Velocity redistribution; Wake flow; Water jets.

1. INTRODUCTION

In large dams, bottom outlets are commonly used for reservoir drawdown, sediment flushing, river diversion and environmental flow releases (e.g. Vischer and Hager 1998, Novak et al. 2001). A typical example is a bottom outlet when a high-velocity supercritical flow discharges past an abrupt drop (Fig. 1). Such high-velocity free-surface flows are extremely turbulent flows, and interfacial aeration is commonly observed. In Fig. 1, the flow Reynolds number is about 8 E+8. Little research has been conducted systematically in the air-water flow properties of the high-velocity waters discharging at the downstream end of the tunnel (Ervine and FALVEY 1987). Experimental studies of high-velocity water jets discharging into the atmosphere were often limited to visual observations (e.g. Kawakami 1973). Some researchers performed air concentration distribution measurements (e.g. Shi et al. 1983, Low 1986, Chanson 1989, Tseng et al. 1992, Kramer 2004), but limited works included air-water velocity distribution measurements (Chanson 1993, Brattberg et al. 1998).

This paper aims to provide some new understanding of the air-water flow properties in high-velocity water jets discharging past an abrupt drop. New experimental investigations were conducted systematically in the free-jet. The data are compared with analytical solutions of the air bubble diffusion equation and with a wake flow model. The results provide new insights into the interactions between the high-velocity water jet and the surrounding air.

2. EXPERIMENTAL SETUP

New experiments were performed in a 0.25 m wide channel ending with a free overfall (Table 1). The flume was equipped with a 0.143 m high step located 0.62 m downstream of a vertical sluice gate. The water flow rates were measured with a V-notch weir calibrated on-site using a volume per time technique. The accuracy on discharge measurements was about 2%. Clear-water depths and velocities were measured with a point gauge and a Prandtl-Pitot tube ($\varnothing$ = 3.3 mm) respectively. Air-water flow properties were measured a double-tip conductivity probe ($\varnothing$ = 0.025 mm) developed at the University of Queensland. The probe tips were aligned in the flow direction and excited by an air bubble detector (AS25240). The resistivity probe signals were scanned for 40 s at 40 kHz per sensor. The translation of the probes in the vertical direction was controlled by a fine adjustment travelling mechanism connected to a Mitutoyo^{TM} digimatic scale unit. The error on the vertical position of the probe was less than $\Delta z < 0.025$ mm. The system (probe and travelling mechanism) was mounted on a trolley system. The accuracy on the longitudinal position of the probe was estimated as $\Delta x <$ 0.5 cm. The accuracy on the transverse position of the probe was estimated as $\Delta y < 0.5$ mm. Further information and details were provided in Toombes (2002).

2.1 APPROACH FLOW CONDITIONS

In the main channel, the approach flow was controlled by a sluice gate. The measured contraction ratio was 0.66 (±5%) in average. The inflow conditions were supercritical : i.e., $2 \leq Fr_o \leq 10$ where Fr_o is the approach flow Froude number. At the abrupt drop, the flow was partially-developed with δ/d_o = 0.21 to 0.35 where δ is the measured boundary layer thickness and d_o is the approach flow depth. The depth-averaged air concentration $(C_{mean})_o$ ranged from 0.02 to 0.04 for the investigated flow conditions, where C_{mean} is defined in terms of 90% air concentration. Nappe ventilation was performed with sidewall offsets. Cavity pressure measurements demonstrated atmospheric pressures within 0.1 mm of water.

Fig. 1 Photographs of air-water flow at bottom outlet - Three Gorges Project on 20 October 2004, V_o = 35 m/s, Q = 1700 m^3/s per outlet, W_o = 9 m (per outlet)

Table 1. Experimental flow conditions

Ref.	x_o m	h m	W_o m	W m	q m^2/s	d_o m	Re	Comments
(1)	(2)	(3)	(4)	(5)	(6)	(7)	(8)	(9)
Present study	0.62	0.1433	0.237	0.250				Perspex step and glass flume.
					0.084	0.0306	3.3 E+5	Run DT1.
					0.097	0.0290	3.9 E+5	Run DT2.
					0.111	0.0296	4.4 E+5	Run DT3.
					0.087	0.0243	3.5 E+5	Run DT4.
					0.143	0.0397	5.7 E+5	Run DT5.

Notes: d_o : approach flow depth; h : step height; Re : Reynolds number defined in terms of hydraulic diameter; W : downstream channel width; W_o : approach channel width; x_o : approach channel length.

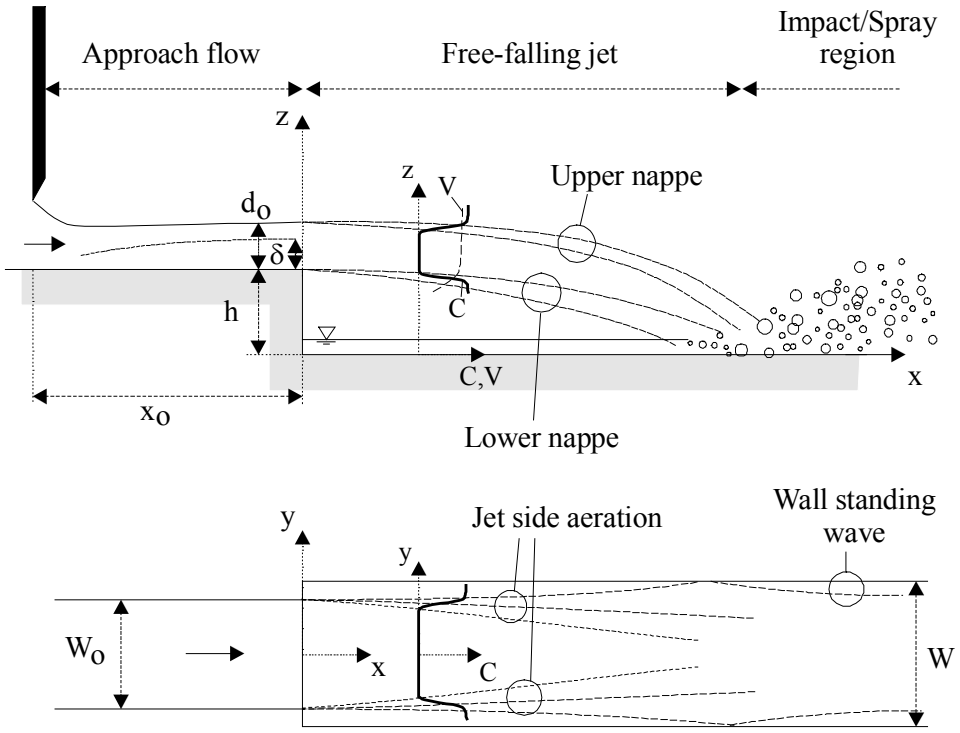

Fig. 2 Definition sketch

3. EXPERIMENTAL RESULTS

For all investigated conditions, the flow may be divided into a number of regions that display distinctive characteristics : i.e., the approach flow, free-falling jet, impact region and a large air cavity (Fig. 2). The flow was associated with significant air entrainment, which may be the cumulative result of a number of mechanisms: (a) interfacial aeration in the approach flow region, and at the upper nappe of the free-jet, (b) bubble entrainment in the developing air-water shear layer at the lower nappe, (c) interfacial aeration along the jet side shear layers, (d) plunging jet entrainment where the lower surface of the free-jet impacts into the pool of water beneath the nappe and (e) flow fragmentation at the impact of the nappe on the downstream invert, resulting in a significant volume of spray. Herein, this study are focused on the first three mechanisms. Toombes (2002) discussed the other mechanisms.

At the lower nappe, an air-water free-shear layer developed downstream of the step brink. Experimental data showed that the amount of air entrained at the lower interface increased with distance from the step edge. At the upper interface, aeration was a combination of bubble entrainment in the air-water shear layer generated by the upstream sluice gate, free surface aeration, and roughness of the free-surface. Although the amount of air entrainment increased slightly with distance from the drop, a slower rate was observed at the upper nappe compared to the lower nappe. Air was entrained into the jet not only at both upper and lower jet interfaces, but as well as along the sides.

At the upper and lower nappes, the air concentration distributions were successfully compared with an analytical solution of the diffusion equation for air bubbles :

$$C = \frac{1}{2} * \left(1 + \text{erf}\left(\frac{z - z_{50}}{2 * \sqrt{D_t * \frac{x}{V_o}}} \right) \right) \quad \text{Upper nappe} \qquad (1a)$$

$$C = \frac{1}{2} * \left(1 + \text{erf}\left(\frac{z_{50} - z}{2 * \sqrt{D_t * \frac{x}{V_o}}} \right) \right) \quad \text{Lower nappe} \qquad (1b)$$

where C is the air concentration, x is the longitudinal distance from the drop, V_o is the approach flow velocity, D_t is the turbulent diffusivity assumed independent of the normal direction z, z_{50} is the location where C = 0.5, and erf is the Gaussian error function. Equation (3) is compared with present data in Figure 3, where Z" = $(z-z_{50})/(z_{90}-z_{10})$, z_{10} and z_{90} are the locations where C = 0.10 and 0.90 respectively, and X is the dimensionless horizontal distance from the drop ($X = x/d_o$). The good agreement between data and theory indicate that D_t was approximately constant at each cross-section, but experimental results showed that D_t increased with increasing distance from the brink. The trend was consistent with a re-analysis of the data of Low (1986), Chanson (1989) and Brattberg et al. (1998). The findings showed that the turbulent diffusivity was best correlated by :

$$\frac{D_t}{\nu} = K * We_X \qquad \text{Lower nappe } (3\text{ E+3} < We_X < 8\text{ E+5}) \qquad (2)$$

where ρ and ν are the water density and kinematic viscosity respectively, We_X is the longitudinal Weber number defined as $We_X = \rho * V^2 * x/\sigma$, V is the air-water velocity, σ is the surface tension between air and water. The majority of the data formed a band between : 1 E-3 < K < 3 E-3, with a mean value of K = 1.5 E-3, despite some scatter accounting for the differences in experimental flow conditions and geometries.

Typical bubble count rate distributions on the jet centreline are shown in Fig. 4. The bubble count rate F_a is the number of air-bubbles or air-structures striking the leading probe tip per second. The data showed systematically maxima in the upper and lower nappe. At the lower nappe, the maximum count rates were about three to five times greater than those observed at the upper interface. Further the maximum bubble count rate F_{max} decreased with increasing distance from the step brink. For all investigated flow rates, the data were best correlated by:

eq \f(σ * F\s\do3(max),ρ * V\s\up5(3)) = \(0.11 * We\s\do3(x) + 610)\s\up5(-1)

Lower nappe (3)

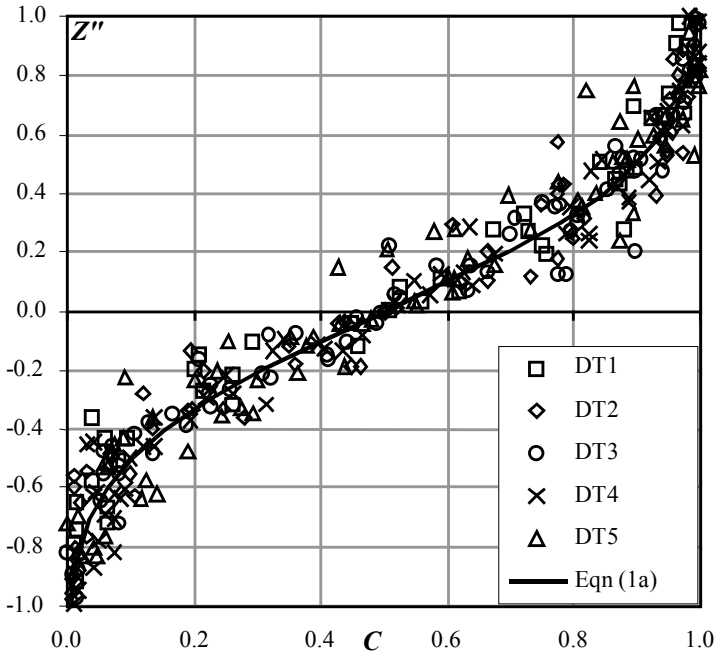

(A) Upper nappe data - Comparison with Equation (1a)

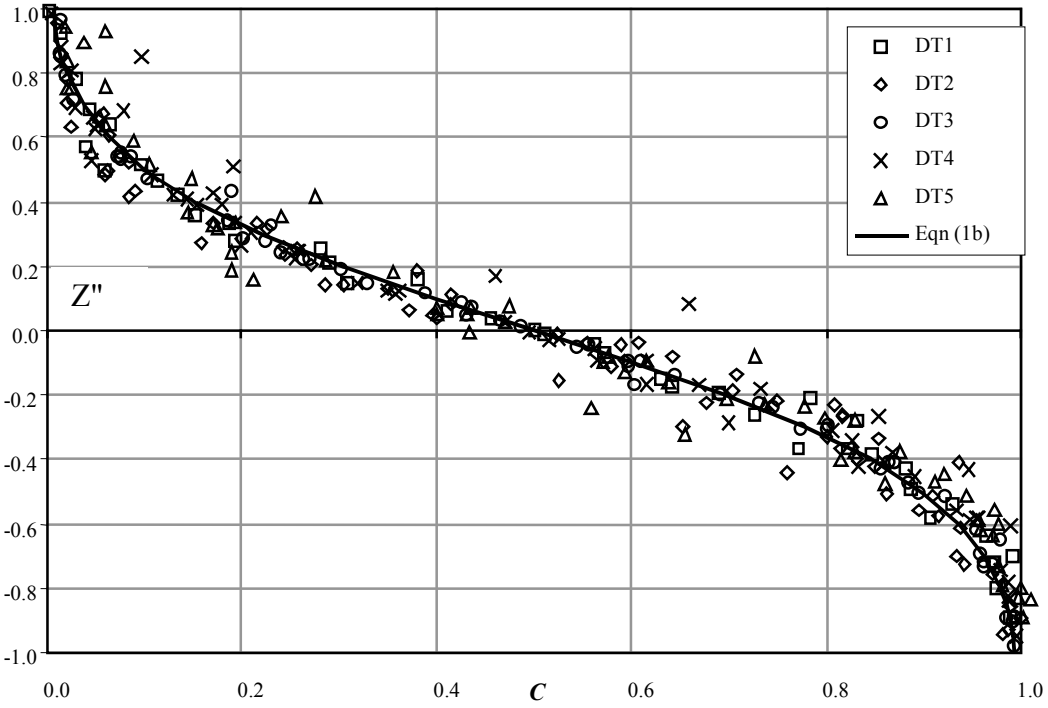

(B) Lower nappe data - Comparison with Equation (1b)

Fig. 3 Dimensionless air concentration distributions (centreline data)

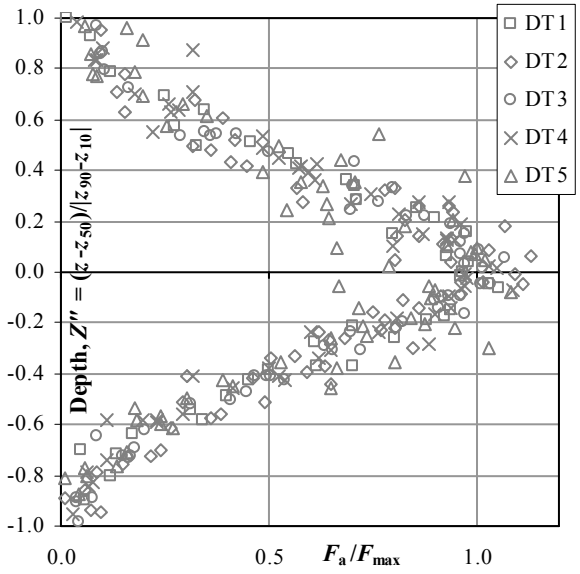

Fig. 4 Dimensionless distributions of bubble count rate at the lower jet interface

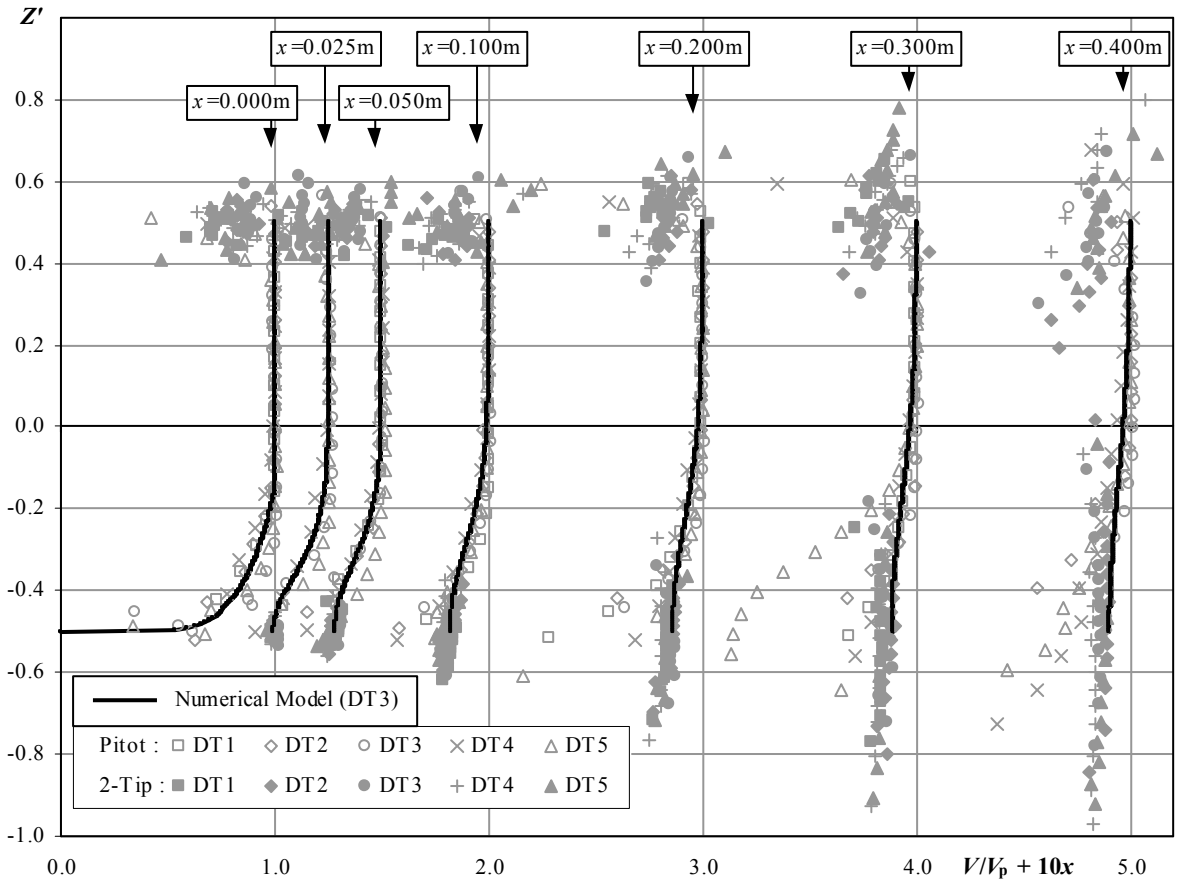

Fig. 5 Dimensionless velocity distributions through the free-jet - Comparison between experimental data and numerical analysis

Typical centreline velocity profiles through the free jet are shown in Figure 5, where V_p is the velocity of the potential (uniform) flow region of the jet, x is measured in metres, Z' is the dimensionless distance centred about a point midway between the points of 50% air concentration at the upper and lower interfaces : $Z' = (z - (z_{50}^{UpperNappe} + z_{50}^{LowerNappe})/2)/d_o$. Data from both double-tip conductivity probe and Pitot tube are shown in Figure 5. At the upper air-water interface, there was negligible momentum exchange between the flow and the atmosphere (Toombes 2002). The inflow conditions were partially-developed with a 'potential' flow region above the boundary layer. This ideal-fluid flow region was maintained in the upper layer of the free-jet, with the velocity increasing along the jet due to gravitational acceleration. The ideal fluid flow velocity was predicted using the Bernoulli equation and the equations of motion with an error of less than 1%. At the lower nappe, the velocity profiles showed a distinct change as the distance from the step brink increased. Immediately downstream of the drop, the velocity profile at the lower interface had a profile similar to that observed in a turbulent boundary layer. The velocity profile became more uniform across the jet as the distance from the drop increased.

For the present investigation, and within the accuracy of the instrumentation, the momentum flux along the water jet J_W ($0 \leq x/d_o \leq 15$) was calculated as :

$$J_W = \int_{z_{90}^{LowerNappe}}^{z_{90}^{UpperNappe}} \rho * (1 - C) * V^2 * dz \quad (4)$$

where V and C are the measured velocity and time-averaged air concentration at elevation z. Calculations based upon experimental data demonstrated that there was basically no loss of momentum from the water jet along its trajectory.

In the approach channel, the turbulent boundary layer was a zone affected by a shearing force from friction at the invert. Downstream of the drop, the shearing force at the lower interface was zero. The internal viscous shear forces within the fluid resulted in a redistribution of the velocity profile along the jet. The continuity and Navier-Stokes equations were numerically integrated, assuming a monophase liquid jet discharging into a void and using Prandtl mixing length hypothesis as: $\tau = \rho * \nu_T * \partial V_x/\partial z$, where V_x is the streamwise velocity component, ν_T is the momentum exchange coefficient assumed independent of z (Goertler 1942). The results demonstrated that the numerical integration predicted well the measured velocity profiles (Toombes 2002). A sample output from the model is shown in Fig. 5. Based upon the measured air-water velocity distributions, the dimensionless momentum exchange coefficient was estimated for the investigated flow conditions to be of the order of $\nu_T/\nu = 400$, where ν is the water kinematic viscosity. Basically the momentum exchange coefficient was found to be independent of the longitudinal location (within $0 \leq X < 15$) and inflow conditions.

3.1 REMARKS

The boundary conditions for a jet of semi-infinite thickness discharging into a void are similar to the boundary conditions for wake flow behind a symmetrical bluff body. Analytical solutions for two-dimensional wake flows can be developed in the far wake region downstream :

$$\frac{V}{V_o} = 1 - \frac{K'}{\sqrt{x}} * \exp\left(-\frac{V_o * z^2}{4 * \nu_T * x}\right) \quad (5)$$

where K' is an integration constant determined to satisfy continuity (e.g. Goertler 1942, Schetz 1993). Equation (5) showed a good agreement with both numerical model and experimental data, although the assumptions upon which Equation (5) is based (i.e. far wake $(1\text{-}V/V_o) \approx 1$), limit the range of the jet over which it can be accurately applied. It must be noted that both analytical and numerical solutions were developed for monophase flow, and they did not implicitly account for interfacial aeration. The output from both models can be adapted to account for air entrainment by adjusting the scaling of the vertical direction as $dz' = dz/(1\text{-}C)$, where z is the vertical coordinate assuming no air entrainment, and z' is the modified coordinate.

4. DISCUSSION

Downstream of the step, the free-jet was subjected to both significant interfacial aeration and velocity redistribution. Close to the step brink ($We_x < 5000$), the air bubble turbulent diffusivity was significantly smaller than the momentum exchange coefficient : i.e., $D_t/\nu_T < 0.02$. The air bubble turbulent diffusivity increased however with distance from the step brink. Consequently, further downstream ($5\ E{+}3 < We_x < 5\ E{+}4$), the turbulent diffusivity was almost of the order of magnitude of the eddy viscosity: $D_t/\nu_T \sim 0.2$ to 0.5. A re-analysis of existing data, presented in Chanson (1997), derived the ratio of turbulent diffusivity to eddy viscosity for a range of experiments, including two-dimensional plunging jets, two-dimensional water jets and open channel flows. Results were typically of the order $0.2 < D_t/\nu_T < 3$. That is, present results for $We_x > 5\ E{+}3$ fall within this range. The ratio of bubble diffusivity to eddy viscosity D_t/ν_T compares the effects of the difference in diffusion of a discrete bubble particle and small coherent fluid structure, as well as the effect of entrained air on the turbulence field. Close to the step brink ($We_x < 5000$), present result (i.e. $D_t/\nu_T < 0.02$) seem to suggest that momentum exchange processes are dominant. Further downstream ($5\ E{+}3 < We_x < 5E{+}4$), the results (i.e. $D_t/\nu_T \sim 0.2$ to 0.5) imply strong competition between the air bubble diffusion and momentum exchange processes. The presence of large amounts of entrained air is expected to modify some turbulence characteristics while the turbulence controls the mechanism of bubble break-up and the air-water interfacial properties.

There were a number of issues regarding both the estimate of the momentum exchange coefficient and any comparison between $_T$ and D_t that had to be considered. These included that measurements of mixing layer width were complicated by the effect of the initial boundary layer velocity profile at the step brink. The thickness of the developing boundary

layer did not necessarily reflect the width of the mixing layer, while the eddy viscosity was not necessarily constant across the boundary layer. Further estimates of turbulent shear stresses and momentum exchange coefficient did not account for air entrainment at the lower interface. It could possibly be argued that the estimate of mixing layer thickness used in the calculations above underestimated (or overestimated) the mixing layer thickness, while the effects of air entrainment on the eddy viscosity were unknown. Additionally the air-water mixing layer thickness was initially significantly less than the width of the momentum mixing layer, but increased significantly with distance from the step brink. The increase in the width of the air-water mixing layer relative to the momentum mixing layer was likely responsible for the growth in D_t observed.

5. SUMMARY AND CONCLUSION

Air entrainment and velocity redistribution were investigated experimentally in a high-velocity flow past an abrupt drop (Figs. 1 and 2). Downstream of the abrupt drop, the free-jet entrained air at both upper and lower air-water interfaces, as well as along the sides. An air-water shear layer developed at the lower nappe interface. Measured air-concentration distributions within the shear layer showed good agreement with an analytical solution of the basic diffusion equation for air-bubbles, based on the continuity equation for air (Eq. (1)). The turbulent boundary layer upstream of the step brink was partially developed. Downstream of the brink, friction forces from the step invert were no longer present and the velocity field at the lower nappe was subjected to a strong redistribution. Experimental results showed a negligible loss of momentum from the free-falling jet to the surrounding air. The velocity redistribution within the jet was successfully modelled by integrating numerically the Navier-Stokes and continuity equations. Beyond a certain distance from the step brink, the velocity field was found to be similar to that in two-dimensional wake flow.

The results highlighted two distinct flow regions. Close to the brink ($We_X < 5000$), the flow was dominated by momentum transfer as the result of the step brink singularity. Further downstream ($We_X > 5000$), the results implied a strong competition between air bubble diffusion and momentum exchanges.

REFERENCES

Brattberg, T., Chanson, H., and Toombes, L. (1998). "Experimental Investigations of Free-Surface Aeration in the Developing Flow of Two-Dimensional Water Jets." *Jl of Fluids Eng.*, Trans. ASME, Vol. 120, No. 4, pp. 738-744.

Chanson, H. (1989). "Study of Air Entrainment and Aeration Devices." *Jl of Hyd. Res.*, IAHR, Vol. 27, No. 3, pp. 301-319.

Chanson, H. (1993). "Velocity Measurements within High Velocity Air-Water Jets." *Jl of Hyd. Res.*, IAHR, Vol. 31, No. 3, pp. 365-382 & No. 6, p. 858.

Chanson, H. (1997). "Air Bubble Entrainment in Free-Surface Turbulent Shear Flows." *Academic Press*, London, UK, 401 pages.

Dodu, J. (1957). "Etude de la Couche Limite d'Air autour d'un Jet d'Eau à Grande Vitesse." *Proc. 7th IAHR Congress*, Lisbon, Portugal, paper D6.

Ervine, D.A., and FALVEY, H.T. (1987). "Behaviour of Turbulent Water Jets in the Atmosphere and in Plunge Pools." *Proc. Instn Civ. Engrs., London*, Part 2, Mar. 1987, 83, pp. 295-314. Discussion : Part 2, Mar.-June 1988, 85, pp. 359-363.

Goertler, H. (1942). "Berechnung von Aufgaben der freien Turbulenz auf Grund eines neuen Näherungsansatzes." *Z.A.M.M.*, 22, pp. 244-254 (in German).

Henderson, F.M. (1966). "Open Channel Flow." *MacMillan Company*, New York, USA.

Heraud, D. (1966). "Dispersion des Jets Liquides; Influence des Rugosités de Paroi." *Ph.D. thesis*, University Grenoble 1, France.

Kawakami, K. (1973). "A Study of the Computation of Horizontal Distance of Jet Issued from Ski-Jump Spillway." *Proc. JSCE*, Vol. 219, No. 11, pp. 37-44 (in Japanese).

Kramer, K. (2004). "Development of Aerated Chute Flow." Ph.D. Thesis, VAW, ETH-Zürich, Switzerland, 178 pages.

Low, H.S. (1986). "Model Studies of Clyde Dam Spillway aerators." *Research Report No. 86-6*, Dept. of Civil Eng., Univ. of Canterbury, Christchurch, New Zealand.

Novak, P., Moffat, A.I.B., Nalluri, C., and Narayanan, R. (2001). "Hydraulic Structures." *Spon Press*, London, UK, 3rd edition, 666 pages.

Rouse, H. (1936). "Discharge Characteristics of the Free Overfall." *Civil Engineering*, Vol. 6, April, p. 257.

Schetz, J.A. (1993). "Boundary Layer Analysis." *Prentice Hall*, Englewood Cliffs, USA.

Shi, Q., Pan, S., Shao, Y., and Yuan, X. (1983). "Experimental Investigation of Flow Aeration to prevent Cavitation Erosion by a Deflector." *Shuili Xuebao* (Jl of Hydraulic Engrg.), Beijing, China, Vol. 3, pp. 1-13 (in Chinese).

Toombes, L. (2002). "Experimental Study of Air-Water Flow Properties on Low-Gradient Stepped Cascades." *Ph.D. thesis*, Dept of Civil Engineering, The University of Queensland.

Tseng, L.K., Ruff, G.A., and Faeth, G.M. (1992). "Effects of Gas Density on the Structure of Liquid Jets in Still Gases." *AIAA Jl*, Vol. 30, No. 6, pp. 1537-1544.

Vischer, D., and Hager, W.H. (1998). "Dam Hydraulics." *John Wiley*, Chichester, UK, 316 pages.